

S-fraction multiscale finite-volume method for spectrally accurate wave propagation

Vladimir Druskin, Alexander V. Mamonov* and Mikhail Zaslavsky, Schlumberger

SUMMARY

We develop a method for numerical time-domain wave propagation based on the model order reduction approach. The method is built with high-performance computing (HPC) implementation in mind that implies a high level of parallelism and greatly reduced communication requirements compared to the traditional high-order finite-difference time-domain (FDTD) methods. The approach is inherently multiscale, with a reference fine grid model being split into subdomains. For each subdomain the coarse scale reduced order models (ROMs) are precomputed off-line in a parallel manner. The ROMs approximate the Neumann-to-Dirichlet (NtD) maps with high (spectral) accuracy and are used to couple the adjacent subdomains on the shared boundaries. The on-line part of the method is an explicit time stepping with the coupled ROMs. To lower the on-line computation cost the reduced order spatial operator is sparsified by transforming to a matrix Stieltjes continued fraction (S-fraction) form. The on-line communication costs are also reduced due to the ROM NtD map approximation properties. Another source of performance improvement is the time step length. Properly chosen ROMs substantially improve the Courant-Friedrichs-Lewy (CFL) condition. This allows the CFL time step to approach the Nyquist limit, which is typically unattainable with traditional schemes that have the CFL time step much smaller than the Nyquist sampling rate.

INTRODUCTION

Seismic inversion requires simulating of acoustic or elastic wave propagation on a very large scale. The computational cost of the forward problem is typically the dominant part of the overall inversion cost. Thus, fast and accurate wave propagation solvers capable of handling large models are of utmost importance. This is particularly true for the iterative inversion techniques such as the full waveform inversion (FWI), which require multiple forward solves at each iteration to compute the minimization functional and its derivative information.

For maximum performance the method must be easily parallelizable. We achieve this by splitting the computational domain Ω into the subdomains Ω^α . This is illustrated in Figure 1 for a 2D case. The derivations and the numerical examples below are for the full 3D case.

On each subdomain Ω^α we discretize the spatial operator on a fine reference grid. The resulting semi-discrete second order wave equation is

$$u_{tt}^\alpha = \mathbf{A}^\alpha u^\alpha, \quad (1)$$

where u^α is the wave field at the fine grid nodes of the subdomain Ω^α . Our framework provides a unified treatment for both the acoustic and elastic cases, so that we do not specify here the exact form of the fine grid discrete spatial operator

$\mathbf{A}^\alpha \in \mathbb{R}^{N \times N}$. The required boundary conditions are embedded into \mathbf{A}^α as needed.

Our method consists of two stages. The first stage is performed off-line before the time stepping. During this stage, the reduced order models are computed for each \mathbf{A}^α . Because there is no interaction between the subdomains at this point, the ROMs are computed in parallel.

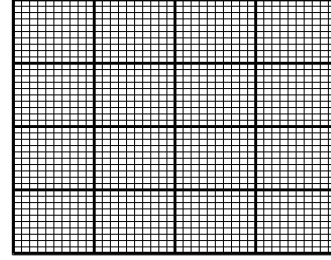


Figure 1: Computational domain Ω with the reference fine grid (thin lines) split into 4×4 subdomains Ω^α with the boundaries $\mathcal{B}^{\alpha\beta}$ (thick lines).

The second stage is the time stepping. At this stage, the adjacent subdomains exchange the information with each other at every time step. To maximize the overall performance, the ROMs constructed earlier should reduce the amount of communication and make the time-step increase possible.

The method presented here is an extension of the techniques of (Druskin and Knizhnerman, 2000; Asvadurov et al., 2000), where the so-called optimal (spectrally matched) grids were used to construct the ROMs on the subdomains. The use of optimal grids relies on the medium being uniform on each subdomain. The method presented here avoids this limitation and allows for arbitrary sharp discontinuities within the subdomains.

STAGE 1: REDUCED ORDER MODELS

The two adjacent subdomains Ω^α and Ω^β communicate only through the shared boundary $\mathcal{B}^{\alpha\beta}$. For a second order PDE all the exchanged information can be captured in a Neumann-to-Dirichlet (NtD) map. Thus, the ROM must approximate well the NtD map while reducing the number of degrees of freedom shared by the subdomains. To achieve this we choose first a small number m of basis functions, columns of $\mathbf{F}^{\alpha\beta} \in \mathbb{R}^{N \times m}$, that are localized on $\mathcal{B}^{\alpha\beta}$ and are zero elsewhere in Ω^α .

Let us denote by $\mathcal{N}(\alpha)$ the indices of the subdomains adjacent to Ω^α . Then, we can combine all six sets (a 3D box has 6 faces) of basis functions $\mathbf{F}^{\alpha\beta}$, $\beta \in \mathcal{N}(\alpha)$ into one matrix $\mathbf{F}^\alpha \in \mathbb{R}^{N \times 6m}$. Transforming (1) to the frequency domain

$$\mathbf{A}^\alpha u^\alpha + \omega^2 u^\alpha = 0, \quad (2)$$

S-fraction multiscale finite-volume method

we can write the frequency-dependent NtD map projected on the basis functions \mathbf{F}^α as

$$\mathbf{M}^\alpha(\omega) = [\mathbf{F}^\alpha]^* (\mathbf{A}^\alpha + \omega^2 \mathbf{I})^{-1} \mathbf{F}^\alpha, \quad (3)$$

which has the exact form of a transfer function of a multi-input/multi-output (MIMO) dynamical system with both inputs and outputs given by \mathbf{F}^α . Hereafter we omit the subdomain index α unless there are more than two subdomains under consideration at once.

Once the NtD map is expressed in the form (3), we can apply the well-developed theory of model order reduction to come up with a ROM

$$\tilde{\mathbf{M}}(\omega) = \tilde{\mathbf{F}}^* (\tilde{\mathbf{A}} + \omega^2 \mathbf{I})^{-1} \tilde{\mathbf{F}}, \quad (4)$$

where $\tilde{\mathbf{A}} \in \mathbb{R}^{6mn \times 6mn}$ and $\tilde{\mathbf{F}} \in \mathbb{R}^{6mn \times 6m}$ with $6mn \ll N$. The ROM has a block structure with n being the number of blocks, as described below.

To obtain high (spectral) accuracy of the resulting numerical scheme, we require $\tilde{\mathbf{M}}(\omega)$ to be a good approximation of the NtD map $\mathbf{M}(\omega)$ as a function of ω . The existing literature contains many approaches to this problem. A large family of approaches uses projection onto some subspace of \mathbb{R}^N to obtain (4). If the columns of some $\mathbf{V} \in \mathbb{R}^{N \times 6mn}$ form an orthonormal basis for the desired projection subspace, the ROM is defined by

$$\tilde{\mathbf{A}} = \mathbf{V}^* \mathbf{A} \mathbf{V}, \quad \tilde{\mathbf{F}} = \mathbf{V}^* \mathbf{F}. \quad (5)$$

A popular choice of a projection subspace is a block (rational) Krylov subspace given by

$$\mathcal{K}_n(\sigma) = \text{colspan} \left\{ (\mathbf{A} + \sigma_1 \mathbf{I})^{-1} \mathbf{F}, \dots, (\mathbf{A} + \sigma_n \mathbf{I})^{-1} \mathbf{F} \right\}, \quad (6)$$

where the shifts σ_j are distinct or repeated, finite or infinite. Here, we use the simplest choice $\sigma_1 = \sigma_2 = \dots = \sigma_n = 0$, which yields a subspace

$$\mathcal{K}_n(0) = \text{colspan} \left\{ \mathbf{A}^{-1} \mathbf{F}, \mathbf{A}^{-2} \mathbf{F}, \dots, \mathbf{A}^{-n} \mathbf{F} \right\}, \quad (7)$$

that can be obtained by applying a block Lanczos iteration to $(\mathbf{A}^{-1}, \mathbf{F})$. Note that the computation of the basis for $\mathcal{K}_n(0)$ requires multiple linear solves with the matrix \mathbf{A} . This is where the bulk of the computational cost of the first stage originates. However, it is alleviated by several factors. First, the computation is only done on small subdomains. Second, the computations for different subdomains are independent of each other, thus they can be performed in parallel. Third, the computation only must be done once before the time stepping. Also, a precomputed Cholesky factorization can be reused for the repeated linear solves. Note that unlike the ROM wave propagation scheme of (Pereyra and Kaelin, 2008), our computation of \mathbf{V} is also independent of the number or position of sources and receivers.

Projection subspace (7) is easy to implement and it provides good accuracy solutions, as shown in the numerical experiments below. However, it may not be optimal in terms of the number of degrees of freedom per wavelength and the possible

improvement of the CFL conditions. Other model reduction techniques such as time- and/or frequency-limited balanced truncation (Gugercin and Antoulas, 2004) are more appropriate for these purposes. Integration of these approached into our framework remains a topic of future research.

Although the size of the reduced order spatial operator matrix $\tilde{\mathbf{A}}$ is much smaller than N , the size of \mathbf{A} , in general it is a dense matrix. In contrast, being a discretization of a differential operator \mathbf{A} is typically very sparse. Since the time stepping involves matrix-vector multiplications with $\tilde{\mathbf{A}}$, the number of non-zero entries is more important for the computational cost than the size of the matrix. We show in the next section how $\tilde{\mathbf{A}}$ can be sparsified without affecting $\tilde{\mathbf{M}}(\omega)$. This construction also plays an important role in coupling the adjacent subdomains for the proper exchange of information at the time-stepping stage.

STAGE 2: TIME STEPPING

Once the ROMs are computed for all the subdomains, the time stepping can be performed with the reduced order spatial operators $\tilde{\mathbf{A}}$. To formulate the coupling conditions for the adjacent subdomains and also to sparsify $\tilde{\mathbf{A}}$ we transform them to a special block tridiagonal form.

Transformation to the block tridiagonal form can be done by applying a block version of the Lanczos iteration to the pair $(\tilde{\mathbf{A}}, \tilde{\mathbf{F}})$ to obtain a unitary $\mathbf{Q} \in \mathbb{R}^{6mn \times 6mn}$ such that

$$\mathbf{T} = \mathbf{Q}^* \tilde{\mathbf{A}} \mathbf{Q}, \quad \mathbf{R} = \mathbf{Q}^* \tilde{\mathbf{F}} = [\mathbf{B}_1, 0, 0, \dots, 0]^*, \quad (8)$$

where \mathbf{T} is a Hermitian block tridiagonal matrix with Hermitian blocks $\mathbf{A}_j \in \mathbb{R}^{6m \times 6m}$ on the main diagonal and $\mathbf{B}_j \in \mathbb{R}^{6m \times 6m}$ on super/sub-diagonals. Unitarity of \mathbf{Q} guarantees that the transformed transfer function

$$\tilde{\mathbf{M}}(\omega) = \mathbf{R}^* (\mathbf{T} + \omega^2 \mathbf{I})^{-1} \mathbf{R}, \quad (9)$$

is exactly the same as (4).

An alternative expression is available for (9) that makes apparent the connection to finite-difference schemes. If we apply the unitary transformation \mathbf{VQ} to (2) then taking into account the tridiagonal structure of \mathbf{T} , we can write

$$\begin{aligned} \mathbf{A}_1 \mathbf{W}_1 + \mathbf{B}_2 \mathbf{W}_2 + \omega^2 \mathbf{W}_1 &= \mathbf{B}_1, \\ \mathbf{B}_j \mathbf{W}_{j-1} + \mathbf{A}_j \mathbf{W}_j + \mathbf{B}_{j+1} \mathbf{W}_{j+1} + \omega^2 \mathbf{W}_j &= \mathbf{0}, \end{aligned} \quad (10)$$

for matrices $\mathbf{W}_j \in \mathbb{R}^{6m \times 6m}$, $j = 1, 2, \dots, n+1$, with $\mathbf{W}_{n+1} = \mathbf{0}$. Then using the structure of \mathbf{R} , the expression for the transfer function (9) is simply

$$\tilde{\mathbf{M}}(\omega) = \mathbf{B}_1 \mathbf{W}_1. \quad (11)$$

A second change of coordinates can simplify (11) even further. We can transform (10) to

$$\begin{aligned} \hat{\Gamma}_1 (\Gamma_1 (\mathbf{U}_2 - \mathbf{U}_1)) + \omega^2 \mathbf{U}_1 &= \hat{\Gamma}_1, \\ \hat{\Gamma}_j (\Gamma_j (\mathbf{U}_{j+1} - \mathbf{U}_j) - \Gamma_{j-1} (\mathbf{U}_j - \mathbf{U}_{j-1})) + \omega^2 \mathbf{U}_j &= \mathbf{0}, \end{aligned} \quad (12)$$

S-fraction multiscale finite-volume method

where $U_j \in \mathbb{R}^{6m \times 6m}$, $j = 1, 2, \dots, n+1$, with $U_{n+1} = 0$. The corresponding transformation is done recursively

$$\begin{aligned} \mathbf{G}_{j+1} &= [\mathbf{G}_j^* \mathbf{\Gamma}_j]^{-1} \mathbf{B}_{j+1}, \\ \hat{\mathbf{\Gamma}}_{j+1} &= \mathbf{G}_{j+1} \mathbf{G}_{j+1}^*, \\ \mathbf{\Gamma}_{j+1} &= -\mathbf{G}_{j+1}^* \mathbf{A}_{j+1} \mathbf{G}_{j+1}^{-1} - \mathbf{\Gamma}_j, \\ \mathbf{U}_{j+1} &= \mathbf{G}_{j+1} \mathbf{W}_{j+1}, \end{aligned} \quad (13)$$

starting with $\mathbf{G}_1 = \mathbf{B}_1$, $\mathbf{\Gamma}_0 = 0$. The transfer function is trivial

$$\tilde{\mathbf{M}}(\omega) = \mathbf{U}_1. \quad (14)$$

In 1D, all the quantities in (12)–(13) would be scalars, so the following expression for the transfer function is known to be valid

$$\tilde{M}(\omega) = \frac{1}{\hat{\Gamma}_1^{-1} \omega^2 + \frac{1}{\Gamma_1^{-1} + \frac{1}{\ddots + \frac{1}{\hat{\Gamma}_n^{-1} \omega^2 + \Gamma_n}}}}, \quad (15)$$

which is known as a Stieltjes continued fraction (S-fraction). Thus, our method expresses the 3D NtD map as a matrix generalization of the S-fraction. Note that for a uniform medium in 1D the scalars Γ_j^{-1} , $\hat{\Gamma}_j^{-1}$ are the grid steps of a finite-difference scheme (12) on an optimal (spectrally matched) grid.

Relations (12) provide an easy way to obtain the coupling conditions for the two adjacent subdomains Ω^α and Ω^β . Let us denote by $U_j^\alpha, U_j^\beta \in \mathbb{R}^{6m}$, $j = 1, \dots, n$ the solution vectors on all n “layers” of the ROM. The vectors U_j are related to the solutions u of the original equation (1) by a combined transformation

$$U_j = \mathbf{G}_j [\mathbf{Q}^* \mathbf{V}^* u]_j. \quad (16)$$

To obtain time stepping for the boundary solutions U_1^α we match the solutions and normal fluxes on $\mathcal{B}^{\alpha\beta}$ similarly to finite-volume type methods. These matching conditions applied to (12) imply

$$\begin{cases} \frac{d^2}{dt^2} \left([(\hat{\Gamma}_1^\alpha)^{-1} U_1^\alpha]_\beta + [(\hat{\Gamma}_1^\beta)^{-1} U_1^\beta]_\alpha \right) = \\ \quad [\mathbf{\Gamma}_1^\alpha (U_2^\alpha - U_1^\alpha)]_\beta + [\mathbf{\Gamma}_1^\beta (U_2^\beta - U_1^\beta)]_\alpha, \\ [U_1^\alpha]_\beta = [U_1^\beta]_\alpha \end{cases} \quad (17)$$

where $[X^\alpha]_\beta$ denotes the restriction of X^α on $\mathcal{B}^{\alpha\beta}$.

Note that unless $\hat{\mathbf{\Gamma}}_1^\alpha, \hat{\mathbf{\Gamma}}_1^\beta \in \mathbb{R}^{6m \times 6m}$ are block diagonal with $m \times m$ blocks, equations (17) define a time-stepping scheme for the boundary solutions U_1 with a global mass matrix. This can be avoided by ensuring that the boundary functions on $\mathcal{B}^{\alpha\beta}$ do not overlap for all $\beta \in \mathcal{N}(\alpha)$ and also by adding \mathbf{F}^α to the projection subspace. Then for the shared boundary solution $U_1^{\alpha\beta} = [U_1^\alpha]_\beta = [U_1^\beta]_\alpha$ relations (17) decouple into a scheme

$$\begin{aligned} \frac{d^2 U_1^{\alpha\beta}}{dt^2} &= \left([\hat{\mathbf{\Gamma}}_1^\alpha]_\beta^{-1} + [\hat{\mathbf{\Gamma}}_1^\beta]_\alpha^{-1} \right)^{-1} \times \\ &\quad \times \left([\mathbf{\Gamma}_1^\alpha (U_2^\alpha - U_1^\alpha)]_\beta + [\mathbf{\Gamma}_1^\beta (U_2^\beta - U_1^\beta)]_\alpha \right), \end{aligned} \quad (18)$$

which only requires communication between the adjacent subdomains.

The time stepping for the interior solutions U_j , $j = 2, \dots, n$ is always fully local

$$\frac{d^2 U_j}{dt^2} = \hat{\mathbf{\Gamma}}_j (\mathbf{\Gamma}_j (U_{j+1} - U_j) - \mathbf{\Gamma}_{j-1} (U_j - U_{j-1})). \quad (19)$$

Any standard time stepping scheme can be used for (18)–(19) including Virieux, Runge-Kutta, etc. The expressions on the right hand side of (18)–(19) are always evaluated at the current time step.

METHOD SUMMARY

We summarize below our method as an algorithm that is well suited for parallel HPC platforms.

Algorithm 1 (S-fraction multiscale finite-volume method)

Stage 1. In full parallel mode for each subdomain Ω^α do the following:

- (1.1) Compute the projection subspace bases \mathbf{V}^α and the reduced order models $(\tilde{\mathbf{A}}^\alpha, \tilde{\mathbf{F}}^\alpha)$.
- (1.2) Apply the block Lanczos algorithm to transform $(\tilde{\mathbf{A}}^\alpha, \tilde{\mathbf{F}}^\alpha)$ to a block tridiagonal form $(\mathbf{T}^\alpha, \mathbf{R}^\alpha)$.
- (1.3) Obtain the S-fraction coefficients $\mathbf{\Gamma}_j^\alpha, \hat{\mathbf{\Gamma}}_j^\alpha$ from $(\mathbf{T}^\alpha, \mathbf{R}^\alpha)$ using relations (13)*.
- (1.4) Project the initial conditions $u^\alpha|_{t=0}$ and $\partial_t u^\alpha|_{t=0}$ on the ROM subspace (16) to obtain the initial conditions for U_j^α .

Stage 2. Starting with initial conditions $U_j^\alpha|_{t=0}$ and $\partial_t U_j^\alpha|_{t=0}$ for each time step do the following:

- (2.1) Exchange $[\mathbf{\Gamma}_1^\alpha (U_2^\alpha - U_1^\alpha)]_\beta$ and $[\mathbf{\Gamma}_1^\beta (U_2^\beta - U_1^\beta)]_\alpha$ between the subdomains sharing $\mathcal{B}^{\alpha\beta}$.
- (2.2) While waiting for the data exchange, compute in parallel for each Ω^α the updates to the interior solutions $U_2^\alpha, \dots, U_n^\alpha$ using (19).
- (2.3) Once the data exchange is complete, compute in parallel for each Ω^α the updates to the boundary solutions U_1^α using (18).

Note that the order of steps (2.1) and (2.2) allows for what is known in computer science literature as hiding the communication latency behind the computations. Also, observe that the communication cost is very low. We only exchange vectors of size m between the adjacent subdomains as if we had a second order scheme. In practice the number m of boundary basis functions is chosen based on the source frequency and thus the minimal wavelength of the resulting wavefield. It does not depend on the accuracy of the reference fine grid discretization.

*Steps (1.2) and (1.3) can be combined using a particular form of block Lanczos method.

S-fraction multiscale finite-volume method

This contrasts sharply with the traditional domain decomposition approaches for high order finite-difference schemes, where the communication cost is proportional to the size of the stencil. Such a small communication cost is possible because the ROMs approximate the NtD map to high (spectral) accuracy, even though (12) resemble a three-point difference scheme.

NUMERICAL EXPERIMENTS

We study the viability of our method on a simple numerical example below. We consider an acoustic wave equation

$$u_{tt} = c^2 \Delta u, \quad (20)$$

in a 3D box $\Omega = [0, 7] \times [0, 7] \times [0, 3]$, which is split into $7 \times 7 \times 3$ unit cube subdomains each containing $20 \times 20 \times 20$ reference fine grid nodes. The sizes of ROMs on each Ω^α are $m = 25$, $n = 3$.

The sound speed $c(x, y, z)$ does not depend on z , its dependence on x and y is shown in Figure 2. All the quantities in the example are dimensionless. First order absorbing boundary conditions are enforced on $\partial\Omega$.

The numerical experiment is designed to emphasize the fact that our method allows for the arbitrary placement of the subdomain boundaries relative to the discontinuities of the coefficients of the wave equation. Many subdomains contain one or more discontinuity interfaces of $c(x, y, z)$ including corners. A thin slow fracture of contrast $\max(c)/\min(c) = 10/3$ passes through Ω .

We simulate a single source located at $(3.5, 1.5, 1.5)$ that emits a Gaussian pulse corresponding to a minimal wavelength of $\lambda = 0.78$ for $c = 1$. The solution traces $d(x, t) = u(x, 0, 1.5, t)$ are measured for $t \in [0, 12.5]$. For easier visualization, we normalize the traces by $\int_0^7 d(x, t) dx$ for each $t \in [0.73, 8.2]$ with the results given in Figure 3.

We observe in Figure 3 a good agreement between our method's solution and the solution obtained on a reference fine grid. The relative L_2 norm error between the two is 2.7%. This is achieved with six reduced order degrees of freedom per wavelength per dimension compared to 16 points per wavelength for the fine grid scheme.

CONCLUSIONS AND FUTURE WORK

We performed a first study of a general framework for numerical wave propagation in the time domain using the ROMs in a multiscale setting. In the early numerical experiments the method demonstrated good accuracy while substantially reducing the number of degrees of freedom per wavelength compared to the traditional FDTD schemes. Further improvements in the model order reduction should allow us to approach the Nyquist limit both in space (fewer points per wavelength) and in time (relaxed CFL conditions).

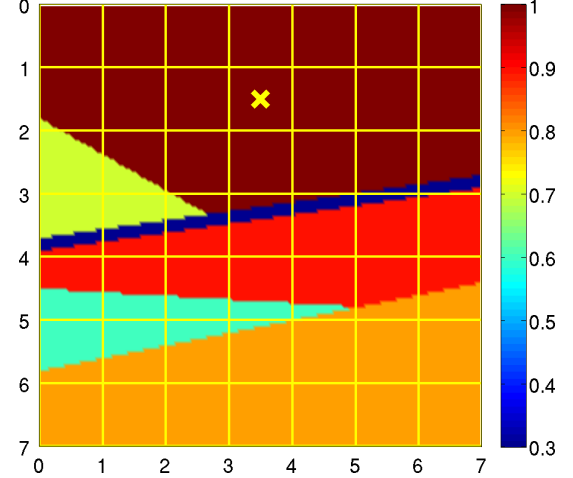


Figure 2: Sound speed profile at $z = 1.5$. Subdomain boundaries are yellow lines, source location is at \times .

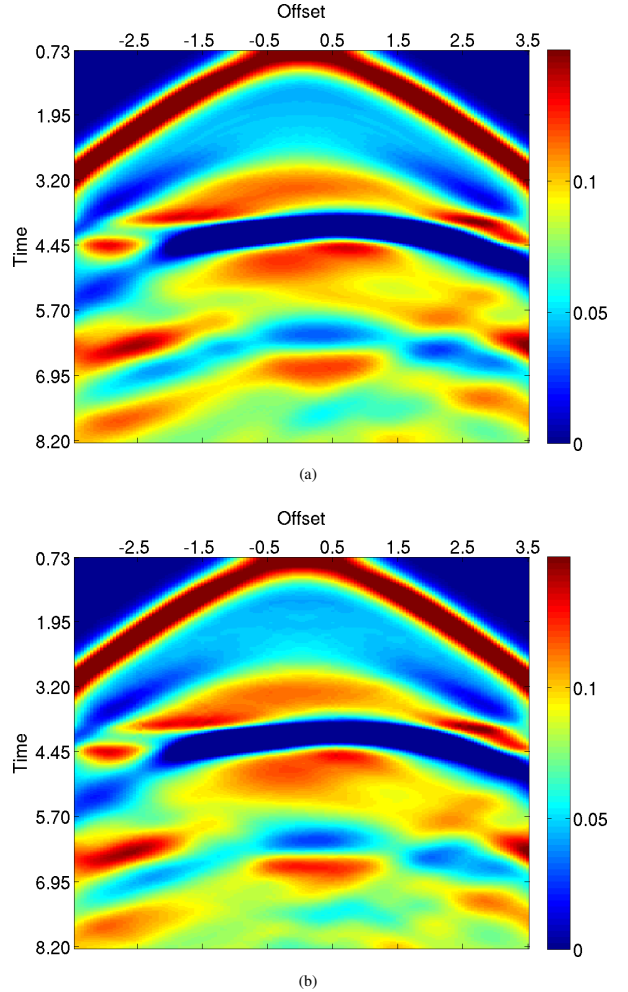


Figure 3: Solution traces at $y = 0, z = 1.5$ normalized for each time for easier visualization: (a) reference fine grid; (b) S-fraction multiscale finite-volume method. Relative error for for $t \in [0, 12.5]$ is 2.7%.

REFERENCES

- Asvadurov, S., V. Druskin, and L. Knizhnerman, 2000, Application of the difference gaussian rules to solution of hyperbolic problems: *Journal of Computational Physics*, **158**, 116–135.
- Druskin, V., and L. Knizhnerman, 2000, Gaussian spectral rules for second order finite-difference schemes: *Numerical Algorithms*, **25**, 139–159.
- Gugercin, S., and A. C. Antoulas, 2004, A survey of model reduction by balanced truncation and some new results: *International Journal of Control*, **77**, 748–766.
- Pereyra, V., and B. Kaelin, 2008, Fast wave propagation by model order reduction: *Electronic Transactions on Numerical Analysis*, **30**, 406–419.